JACS
JOURNAL OF THE AMERICAN CHEMICAL SOCIETY

ARTICLE

pubs.acs.org/JACS

Sequence-Specific Self-Stitching Motif of Short Single-Stranded DNA on a Single-Walled Carbon Nanotube

Daniel Roxbury,[†] Anand Jagota,[†,‡] and Jeetain Mittal*[,†]

[†]Department of Chemical Engineering, and [‡]Bioengineering Program, Lehigh University, Bethlehem, Pennsylvania 18015, United States

Supporting Information

ABSTRACT: The DNA-single-walled carbon nanotube (SWCNT) hybrid molecule has attracted significant attention recently for its ability to disperse and sort SWCNTs according to their chirality. Key for utilizing their unique properties is an understanding of the structure of DNA adsorbed on the SWCNT surface, which we study here using molecular simulations. Using replica exchange molecular dynamics (REMD), we explore equilibrium structures formed by single strands of 12-mer oligonucleotides, of varying sequence, adsorbed on a (6,5)-SWCNT. We find a consistent motif in which the DNA strand forms a right-handed helical wrap around the SWCNT, stabilized by "stitches" (hydrogen bonding between distant bases) to itself. Variability among equilibrium populations of DNA self-stitched structures was observed and shown to be directly influenced by DNA sequence and composition. Competition between conformational entropy and hydrogen bonding between bases is predicted to be responsible for the formation of random versus stitched configurations.

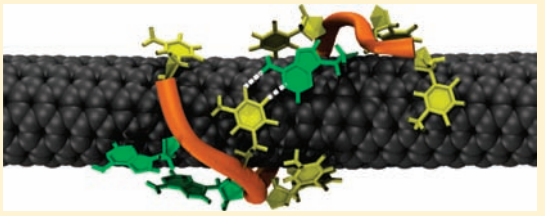

Because of its natural amphiphilic behavior,[1] single-stranded DNA (ssDNA) has been shown, through experimental[2−4] and molecular simulation studies,[5,6] to wrap helically around the outside of single-walled carbon nanotubes (SWCNTs). Hydrophobic DNA bases noncovalently bind to the hydrophobic SWCNT surface through $\pi-\pi$ stacking, with base-dependent binding strengths,[7] while the charge-carrying phosphate−sugar backbone enables dispersion in aqueous medium.[5,8] Novel applications of DNA−SWCNT hybrids have ranged from chemical detection[9,10] to the innate ability to solubilize and sort SWCNTs on the basis of their chirality, length, and diameter.[2,11] Generally, longer DNA sequences (>30 mers) were shown to have higher thermal stability than shorter ones.[12] However, in recent work, Tu et al. have shown that highly sequence-specific short DNA oligomers (10−20 mers), deemed "recognition sequences", can select certain types (chiralities) of SWCNTs from mixtures.[13] This recognition ability of ssDNA has been used to solve a long-standing recalcitrant problem of structure-based sorting of complex mixtures of SWCNTs.[13,14] By quantifying the binding strength through measurement of DNA displacement from the surface of SWCNTs by surfactant molecules, it has been shown experimentally that the addition or subtraction of one base from a recognition sequence strongly affects the relative DNA−SWCNT binding strength,[15] supporting the idea of highly sequence-specific binding. For example, it was found that sequence $(TAT)_4$ (i.e., TATTATTATTAT), being the recognition sequence for the (6,5) chirality SWCNT, binds ∼20 times stronger than either $(TAT)_4T$ or $(TAT)_3TA$. Interestingly, while longer oligonucleotides (>30 mers) bind stronger than shorter ones (e.g., $(TAT)_{10}$ binds an order of magnitude stronger than $(TAT)_4$), they do not show the strong sequence specificity that the shorter ones do.

Molecular simulation has played a significant role in understanding DNA−SWCNT hybrid structures. Previous studies by Johnson et al., involving a long ssDNA (60-mer) near an (11,0)-SWCNT, have shown that spontaneous wrapping occurs when the two species encounter each other.[6] More recently, Johnson et al. modeled the sequence $(GT)_7$ around an (11,0)-SWCNT employing replica exchange molecular dynamics (REMD),[16,17] in an effort to reduce the probability that structures remain trapped in local energy minima.[18] From their ∼100 ns REMD simulation, it was concluded that single strands of DNA can form a variety of structures on the surface of a SWCNT, with no clear preferred state. Furthermore, they have concluded that there is little sequence specificity, and in particular no structure forms that would permit longer-range order (multiple strands). It is difficult to reconcile this proposal with the experimental finding of strong sequence-specific recognition. In a previous study, we examined ordered structures that surface-adsorbed oligonucleotides could assume.[19] In agreement with Johnson et al.,[18] we found that surface-adsorbed strands of ssDNA prefer a motif in which bases alternate from side to side on the backbone, minimizing crowding, and that hydrogen bonding between adsorbed bases on different strands could lead to the emergence of secondary structures. A number of base pair dimers (including non-Watson−Crick base pairs) were studied systematically and used to construct DNA β-barrel structures, leading to the hypothesis that such hydrogen-bonded structures might stabilize an ordered DNA arrangement as the basis for SWCNT recognition. Because only traditional MD simulations were performed for relatively short simulation times (10 ns), no attempt was made to examine equilibrium structures. Here, we present a study on the equilibrium sequence-specific structures arising from one strand binding to an SWCNT. The (6,5)-SWCNT, its recognition sequence,

Received: May 13, 2011
Published: July 28, 2011

$(TAT)_4$, and some related controls were chosen for simulation. The principal questions we wish to examine are as follows: (a) What are the typical motifs in equilibrium? (b) How strongly does the prevalence and population of these motifs depend on DNA composition and sequence?

METHODOLOGIES

All-atom REMD simulations were performed to study the various structures that single strands of ssDNA can form when exposed to a pristine SWCNT surface. As mentioned previously, we chose the (6,5) chirality SWCNT and its hybrid with the (6,5) recognition DNA strand, $(TAT)_4$, for study. As measures of comparison, several other related sequences were examined: A_{12} and T_{12}, and $T_4A_4T_4$. The SWCNT used throughout the entire study was a periodic (6,5) chirality tube, 79.70 Å in length and 7.46 Å in diameter, where end carbons were covalently bonded to adjacent image carbons. For SWCNT force field parameters, we have used standard CHARMM parameters for the sp^2-hybridized carbon atom. Previously, it has been shown that the observed behavior with the CHARMM parameters is consistent with those of Amber-based parameters for CNT[20] as well as for oligonucleotides.[21] All structures were created in Materials Studio,[22] and visualized in VMD.[23]

To run the REMD simulations, the GROMACS 4.5.3 simulation package[24−26] was used with the CHARMM27 force field.[27,28] The DNA strands were initially placed in a left-handed helical configuration with all bases being adsorbed onto the SWCNT sidewall in a backbone-alternating fashion (see Supporting Information section S1). The DNA−SWCNT hybrids were then solvated in a 79.7 × 34.6 × 34.6 Å water box containing approximately 3000 TIP3P model[29] water molecules and sodium counterions, placed randomly, to balance the negative phosphate charges (11 in total), with total system size ∼10 000 atoms. Sodium ions were highly dynamic throughout the simulation and represent a concentration of 191.5 mM, not of unreasonable strength for a DNA buffer. Structures were subjected to 100 ps heating (NVT) to get to 300 K. They were then ready for extended NVT REMD simulation using periodic boundary conditions in all directions with electrostatics calculated using the particle mesh Ewald method (PME).[30] Forty replicas were created for differing DNA sequences, starting in the same initial configuration, having temperatures ranging from 296 to 587 K, with temperature intervals increasing as absolute temperature increased but chosen so that the acceptance ratio remained around 20% with an exchange time of 2 ps. The 40 replicas were then run for 200 ns, for a total computational time of 40 × 200 = 8000 ns. The last 150 ns of each configuration was considered production and used for analysis. The time step of the simulation was 2 fs. The trajectories were saved every 10 ps, yielding a total of 15 000 snapshots for production analysis. For clustering, helicity, and stitching analysis, the room temperature (300 K) replica trajectory was used.

RESULTS AND DISCUSSION

The aromatic nature of DNA bases (sharing of π-orbital electrons) gives rise to their intrinsic hydrophobic tendencies, including the ability to stack on hydrophobic surfaces.[1] Multiple reports have confirmed as much as 10 k_BT/base stacking energies (in water) are experienced when DNA bases adsorb onto a flat hydrophobic surface, such as graphite.[31] Because there is at least one base per Kuhn length (a rigid segment of a freely jointed chain)[32] for oligonucleotides, they are strongly adsorbed, and the entire chain is essentially constrained in the two dimensions of the surface. We have proposed that steric hindrance between adjacent DNA bases promotes conformations in which bases alternate on either side of the backbone. Additionally, bases in such conformations are readily available for hydrogen bonding with other bases.[13,14,19] For 12-mer oligonucleotide chains, it is easy to see that a relatively great amount of energy is required to remove a single chain from such a surface, suggesting that DNA remains bound and selectivity can arise from interactions between adsorbed bases. We therefore hypothesize that the majority of structures will follow the base-alternating motif and that bases will essentially remain stacked onto the SWCNT surface.

First, we investigate the prevalence of the base-alternating motif and base-stacking probabilities for the single-strand $(TAT)_4$−(6,5)-SWCNT hybrid and its close relatives, A_{12}, T_{12}, and $T_4A_4T_4$. We find that 98% of all bases stack onto the SWCNT surface at 300 K, where a base is categorized as stacked when its normal is less than 30° away from the SWCNT normal. Because bases consist of one or two planar aromatic rings, taking the cross-product of two vectors in the plane of the base gives the base normal vector. The SWCNT normal is defined as the outward radial direction. This stacking percentage only varied slightly by DNA composition, for example, 96% for A_{12} to 98% for T_{12}, establishing the expected strong adsorption (see Supporting Information section S2 for detailed results). Phosphorus and base−centroid distance from SWCNT surface were determined to be, on average, 5.92 ± 0.14 and 3.65 ± 0.09 Å, respectively. This did not vary substantially by DNA sequence, confirming the need for the phosphate to be hydrated and away from the SWCNT surface as compared to the base, which stacks onto the SWCNT surface (see Supporting Information section S3). Additionally, the probability that base $i + 1$ is on the opposite side of the backbone from base i was found. Figure 1 presents snapshots of $(TAT)_4$ showing the base−backbone alternating motif, followed by associated probabilities for all of the DNA compositions examined. Note that all strands started with alternating probability of "1". As described later, deviation from this value of 1 leads to emergence of specialized structures.

To observe the underlying conformations associated with one strand REMD simulations, trajectories were grouped into clusters identified by predetermined criteria. In clustering analysis, groups of atoms are compared against others in the trajectory subject to a root mean squared cutoff distance (rmsd), at the same time removing rigid body rotations and translations. Thus, the clustering analysis reveals groups of similar conformations. In our analysis, only positions of the DNA backbone atoms were tracked (phosphate groups and sugar carbons), as this was deemed the most useful of clustering techniques. It was during clustering that we noticed the prevalence of the truly dominant structure. Figure 2 displays the most dominant cluster for $(TAT)_4$, representing 94% of structures, when clustering was performed on the basis of a 0.45 nm backbone rmsd cutoff. Subjected to the same analysis, percentages of the largest clusters were 69%, 90%, and 84%, for $T_4A_4T_4$−, A_{12}−, and T_{12}−SWCNT hybrids, respectively, shown in Supporting Information section S4. The largest clusters all contain DNA in right-handed helical conformations. However, the helical angle, defined as the angle between DNA strand and SWCNT axis, can be noticeably different in a sequence-specific manner (e.g., A_{12} has a distinctly larger helical angle (closer to 90°) than does a sequence like T_{12}). This can be directly related to the degree of DNA−base stitching, as shown later.

We note that all simulations were started with structures in a base-alternating, left-handed helical configuration. All of the examined oligonucleotides alter conformation significantly (including backbone and base placement), and most prefer a right-handed helical conformation about the SWCNT (Figure 2). This strongly suggests that the initial configuration did not affect

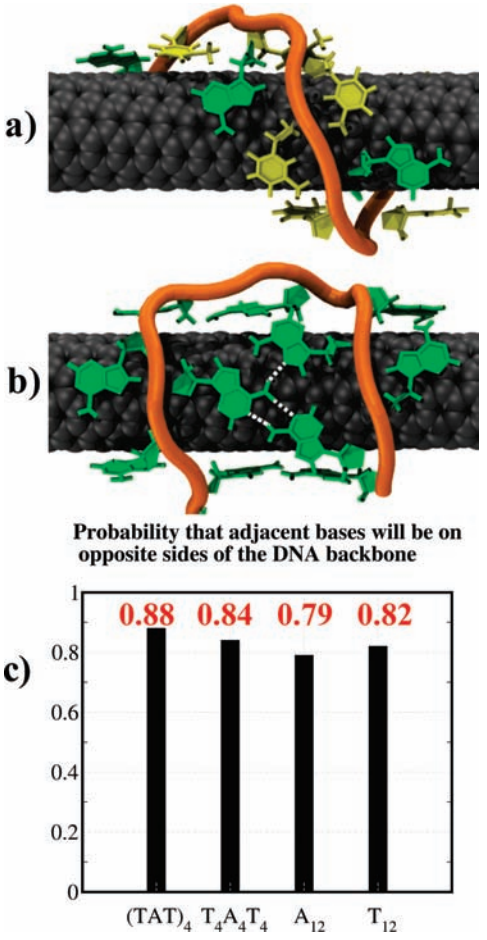

Figure 1. (a) A snapshot of a $(TAT)_4$ strand on (6,5)-SWCNT displaying the base-alternating motif where consecutive bases are on opposite sides of the DNA backbone. Adenine (green) and thymine (yellow) bases participate in base−base hydrogen bonding (white dashed lines). (b) The loop structure found in A_{12}, stabilized by hydrogen bonds (white) between Adenine bases in the interior of the loop. (Water molecules have been removed for clarity.) (c) Comparison of probabilities by DNA composition.

Figure 2. Clustered hybrids of $(TAT)_4$−SWCNTs after being subjected to a 0.45 nm rmsd cutoff of DNA backbone atoms after subtracting rigid body rotations and translations. The backbone atoms of the largest cluster, representing 94% of the trajectory, are shown viewed at strand ends (top) and rotated by 180° to show the middle of the strand (bottom). Note the right-handed helicity of the clustered structures.

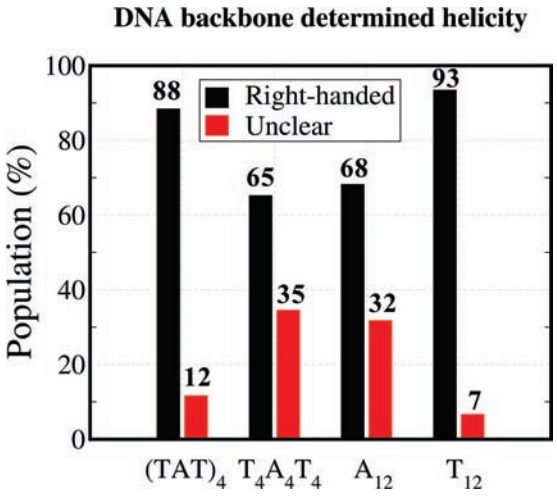

Figure 3. Quantified DNA backbone determined helicity data from all examined sequences. Outlined in the main text, overall DNA helicity (or lack thereof) was calculated on the basis of local helicity between phosphorus atom pairs.

the observed results, which we can take to be representative of equilibrium behavior.

To quantify the DNA helical handedness, phosphorus atom positions were identified and monitored. Any given configuration has 11 phosphorus atoms, that is, 10 adjacent phosphorus pairs. Local helical angles were determined for each phosphorus pair (10 local helical angles per structure). While traversing the SWCNT axis (with increasing axial coordinate), phosphorus pairs determined to be locally right-handed were assigned a "1", else they were assigned a "0" for a locally left-handed helix. Because of the intrinsic DNA−backbone flexibility, a DNA strand with a visibly right-handed overall helical conformation may have a few local left-handed helical angles. Once this binary system was established, the following definition was adopted: If 8 out of 10 local helical angles were assigned "1", the structure was classified as right-handed and vice versa for left-handed. Furthermore, if a structure contained 5 consecutive local helical angles with the designation "1", without previous right-handed classification, it was also delineated as such. The same applies for left-handed if there were 5 in a row with designation "0". Structures not designated either right- or left-handed were termed "unclear" and generally formed a loop structure (Figure 1b). In this way, it was confirmed that right-handed structures prevail in the equilibrium ensemble. Figure 3 shows the sequence dependence of helical handedness. Note that $T_4A_4T_4$ and A_{12} have distinctly lower percentages of structures in a right-handed helical formation. Surprisingly, across all sequences, the population of left-handed helical structures was negligible and has been left out in Figure 3. The relative trends were conserved (insensitive), independent of cutoff values; see Supporting Information section S5. It was found that the initial left- to right-handed helical transition occurred within the first 6−30 ns. Interestingly, DNA passed through a 90° helical angle (oblong loop around SWCNT) rather than becoming outstretched (in the SWCNT axial direction) to accomplish the transformation. Detailed analysis of transition time scales and snapshots are shown in Supporting Information section S6.

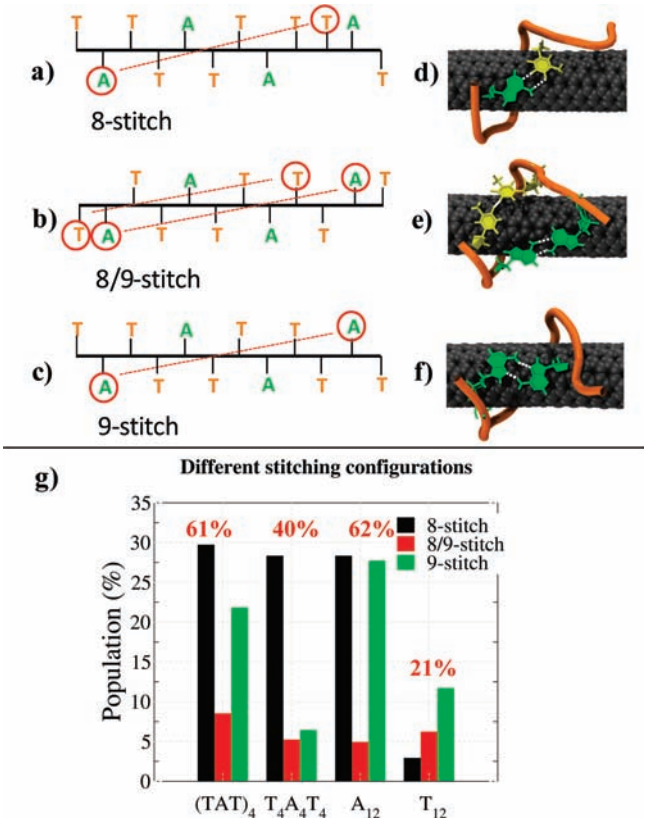

Figure 4. Analysis of REMD conformations shows the emergence of structures comprising a wrapped configuration stabilized by hydrogen bonding between bases at distal ends of the DNA chain. In all cases, three major modes of stitching DNA ends together around a SWCNT were found. The term "8-stitch" refers to a hydrogen bond between one base, and another that is 8 bases away (i and $i + 8$). Shown are illustrations for the 8-stitch, 8/9-stitch, and 9-stitch (a–c) and molecular models taken from actual trajectories (d–f), although these are only representations and not the only conformations possible for each stitch. Stitching populations are also plotted among DNA sequences with total structures stitched found in red (g).

In a previous study of a different sequence/SWCNT combination ($(GT)_7$ on an (11,0)-SWCNT), Johnson et al.[17] found a looplike dominant structure. Our finding of a dominant right-handed helical structure in the $(TAT)_4$–(6,5)-SWCNT hybrid highlights two new points. First, the backbone clustering analysis used in this work was found to be an effective tool to help reveal ordered structures. Second, our result indicates that the DNA/SWCNT hybrid system can have significant structural variation among DNA of varying sequence. Therefore, we can conclude that sequence specificity, in addition to length, is crucial in determining equilibrium structure populations for these short oligomers.

It has been hypothesized that hydrogen bonding plays a critical role in stabilizing DNA–SWCNT structures. In support of this notion, we found that the majority of structures contained at least one hydrogen bond, to stitch the ends of the DNA strands together. To quantify the presence of stitched structures, we define it to occur when a DNA strand makes a complete wrap around a SWCNT allowing distal bases to form at least one hydrogen bond. As shown in a later derivation, stitching itself results in a relatively large loss in DNA conformational entropy, only to be energetically compensated by the formation of a hydrogen bond or bonds. In Figure 4, using $(TAT)_4$ as the representative hybrid, we illustrate the three major types of stitches found in all DNA compositions studied. (Additional details can be found in Supporting Information section S7 for all configurations.) The "8-stitch" refers to a hydrogen bond formed between one base, and another which is 8 nucleotides away (i and $i + 8$). This particular stitch (Figure 4a) requires a base to switch to the opposite side of the backbone, as do all stitches that connect an even numbered separation of nucleotides. We presume that this configuration of three adjacent bases results in some increase in free energy due to crowding, which is more than compensated for by the decrease in free energy due to hydrogen-bond formation, resulting in a stable equilibrium structure. Also possible for 12-mers on (6,5)-SWCNTs are the "9-stitch" and the "8/9-stitch", consisting of both an 8-stitch and a 9-stitch. Figure 4a–c is only representative; that is, there are a number of different conformations with 8- and 9-stitches. For the 8-stitch, A–T stitching is significantly preferred over T–T (60% vs 39%). In the case of the 9-stitch, A–A is highly favored over T–T (95% vs 5%). This highlights the importance of non-Watson–Crick base pairing in stabilizing surface-adsorbed DNA structures.

Although these three stitching forms are found in all DNA compositions ($(TAT)_4$, A_{12}, T_{12}, and $T_4A_4T_4$), their prevalence in each can vary dramatically. As shown in red in Figure 2g, the percentage of structures that stitch depends strongly on the DNA composition and sequence. With the abundance of adenine bases near DNA strand ends, sequences such as $(TAT)_4$ and A_{12} can form the stronger AT and AA hydrogen bonds[33] and have relatively high total stitching percentages (number of structures in trajectory that stitch/total number in trajectory) of 61% and 62%, respectively. Contrary to this, a sequence such as T_{12} has a comparatively low stitching percentage of 21%, consistent with the weaker hydrogen-bond strengths stated above. Also from Figure 4e, DNA sequences with adenine-rich ends show no preference for having either an 8-stitch or a 9-stitch. The sequence, $T_4A_4T_4$, shows a strong preference for an 8-stitch, while T_{12} prefers a 9-stitch, suggesting sequence-specific changes in surface-bound backbone undulations (essentially shortening the P–P distance) allowing for a tighter wrap.

We have previously proposed β-sheet and β-barrel structures formed by hydrogen bonding between (alternating) bases on different strands.[19] However, we neglected the possibility of an ordered structure resulting from the self-hydrogen-bonding, "stitching" motif presented here. In the Supporting Information (section S8), we show the basic geometrical parameters of an ssDNA strand are consistent with the 9-stitch being a favored mode of stitching (given sufficient reduction in free energy due to hydrogen bonding).

It is instructive to consider contributions to the free energy of different conformations to understand the main competing terms that determine whether a stitched structure can be stable. Because we are considering a strongly adsorbed regime, all conformations can be taken to be equally well adsorbed, and the large free energy of adsorption per base no longer plays a role in determining competition between different surface conformations. Instead, we examine the relative contributions of four terms. (a) Hydrogen bonding, the first, favors stitch formation. The remaining three all oppose it and are (b) loss of conformational entropy due to stitch formation, (c) increase in free energy due to enhanced electrostatic repulsion on stitch formation, and (d) increase in free energy due to bending as well as the

penalty for bases switching sides with respect to the backbone to accommodate a certain stitch.

(a) Hydrogen-bond energies have been reported as 10.9 k_BT/bond and 3.4 k_BT/bond in vacuum and fully solvated states.[1,34] Because DNA bases are only half solvated on a SWCNT sidewall, the energy for one bond can be expected to lie between these two values. For simplicity, we can estimate a maximum of about 5.0 k_BT/bond. Because stitched structures are stabilized usually by two hydrogen bonds, this term contributes about $-10\ k_BT$.

(b) Loss of conformational entropy due to stitching is estimated approximately by the work required to pull a 2D Gaussian chain to extension equal to its contour length,[32] because to accommodate a stitch, the DNA must become fully stretched in the two dimensions of the SWCNT surface. Kuhn length, l_k, of short single-stranded DNA has been measured by AFM to be between 0.5 and 1.0 nm;[31] for the present estimations, we take it to be 1.0 nm (corresponding persistence length $l_p = l_k/2 = 0.5$ nm). For a 12-mer, taking the P−P distance to be 0.65 nm, the contour length is 7.15 nm, and therefore the number of Kuhn lengths is about 7. The free energy due to stretching of the backbone can be approximated as

$$G_{conf} = N\ k_BT = 7\ k_BT \quad (1)$$

which is clearly of the same order of magnitude as the hydrogen-bonding term (but of opposite sign).

(c) The electrostatic contribution can be estimated as bending a line of charges to radius of curvature R, which are a defined distance b apart. ΔU_{el} is then defined by charge, q, Debye screening length, l_D, and dielectric constant, ε, as

$$\Delta U_{el} = \frac{q^2 b e^{-b/l_D}}{4\pi\varepsilon\varepsilon_o(24R^2)} \quad (2)$$

from which we estimate (see Supporting Information section S9) the electrostatic contribution to be about

$$\Delta U_{el} \approx 0.1\ k_BT \quad (3)$$

(d) The energy required to bend ssDNA at a radius of 0.98 nm (radius at which phosphorus sits from center of SWCNT axis) is

$$G_{bend} = \frac{l_p l_t k_B T}{2R^2} \approx 0.85\ k_BT \quad (4)$$

where l_p and l_t refer to the DNA persistence[35] and total length, respectively.

When a base switches sides of the backbone, a penalty must be assessed to account for the imposed crowding. Although we do not have an estimate for this contribution, we can assume a small value because all DNA sequences have significant populations of the base−backbone flipping 8-stitch. A snapshot of this conformation is shown in Supporting Information section S10.

This approximate analysis shows that very likely the equilibrium between stitched and random conformations is governed by competition between attractive hydrogen-bonding interaction between bases and attendant reduction in conformational entropy.

CONCLUSIONS

An equilibrium MD study has been presented for short (12-mer) single strands of ssDNA on a particular SWCNT (6,5). We find that some broad characteristics of adsorption onto the SWCNT surface are not sequence dependent. For instance, adsorption is sufficiently strong so that nearly all bases remain stacked on the surface and the backbone usually assumes a right-handed helical conformation with characteristic distance from the SWCNT surface. This finding is consistent with the experimental finding that nearly all DNA sequences are effective dispersants of SWCNTs. However, we find that the actual structural motif of the adsorbed strand depends strongly on the sequence and composition. The basis of the sequence dependence is the highly variable nature of base−base hydrogen bonding, which competes with backbone conformational entropy to result in different, sequence-dependent self-stitched wrapped structures. That is, short strands of DNA, of differing sequence and/or composition, have the ability to form highly sequence-specific structures on SWCNTs. If strands are of adequate length, hydrogen bonding will enable DNA to wrap completely around a SWCNT and self-stitch.

ASSOCIATED CONTENT

Supporting Information. Complete MD analysis of stitching configurations as well as a geometric model and electrostatic free energy contributions. This material is available free of charge via the Internet at http://pubs.acs.org.

AUTHOR INFORMATION

Corresponding Author
jeetain@lehigh.edu

ACKNOWLEDGMENT

This work was supported by the National Science Foundation through grant CMMI-1014960. This research was supported in part by the National Science Foundation through TeraGrid resources provided by the Texas Advanced Computing Center (TACC) under grant number [TG-MCB100049]. We specifically acknowledge the assistance of Mr. Chris Hempel and Dr. Hang Liu.

REFERENCES

(1) Saenger, W. Principles of Nucleic Acid Structure; Springer-Verlag: New York, 1984.
(2) Zheng, M.; Jagota, A.; Strano, M. S.; Santos, A. P.; Barone, P.; Chou, S. G.; Diner, B. A.; Dresselhaus, M. S.; Mclean, S. R. L.; Onoa, G. B.; Samsonidze, G. G.; Semke, E. D.; Usrey, M.; Walls, D. J. *Science* **2003**, *302*, 1545–1548.
(3) Campbell, J. F.; Tessmer, I.; Thorp, H. H.; Erie, D. A. *J. Am. Chem. Soc.* **2008**, *130*, 10648–10655.
(4) Dukovic, G.; Balaz, M.; Doak, P.; Berova, N. D.; Zheng, M.; McLean, R. S.; Brus, L. E. *J. Am. Chem. Soc.* **2006**, *128*, 9004–9005.
(5) Manohar, S.; Tang, T.; Jagota, A. *J. Phys. Chem. C* **2007**, *111*, 17835–17845.
(6) Johnson, R. R.; Johnson, A. T. C.; Klein, M. L. *Nano Lett.* **2008**, *8*, 69–75.
(7) Johnson, R. R.; Johnson, A. T. C.; Klein, M. L. *Small* **2010**, *6*, 31–34.
(8) Zheng, M.; Jagota, A.; Semke, E. D.; Diner, B. A.; Mclean, S. R. L.; Richardson, R. E.; Tassi, N. G. *Nat. Mater.* **2003**, *2*, 338–343.

(9) Barone, P. W.; Baik, S.; Heller, D. A.; Strano, M. S. *Nat. Mater.* **2005**, *4*, 86–92.
(10) Heller, D. A.; Jin, H.; Martinez, B. M.; Patel, D.; Miller, B. M.; Yeung, T. K.; Jena, P. V.; Hobartner, C.; Ha, T.; Silverman, S. K.; Strano, M. S. *Nat. Nanotechnol.* **2008**, *4*, 114–120.
(11) Huang, X.; Mclean, S. R. L.; Zheng, M. *Anal. Chem.* **2005**, *77*, 6225–6228.
(12) Albertorio, F.; Hughes, M. E.; Golovchenko, J. A.; Branton, D. *Nanotechnology* **2009**, *20*, 395101−395109.
(13) Tu, X. M.; Manohar, S.; Jagota, A.; Zheng, M. *Nature* **2009**, *460*, 250–253.
(14) Khripin, C. Y.; Manohar, S.; Zheng, M.; Jagota, A. *J. Phys. Chem. C* **2009**, *113*, 13616–13621.
(15) Roxbury, D.; Tu, X.; Zheng, M.; Jagota, A. *Langmuir* **2011**, *27*, 8282–8293.
(16) Sugita, Y.; Okamoto, Y. *Chem. Phys. Lett.* **1999**, *314*, 141–151.
(17) Sugita, Y.; Kitao, A.; Okamoto, Y. *J. Chem. Phys.* **2000**, *113*, 6042–6051.
(18) Johnson, R. R.; Kohlmeyer, A.; Johnson, A. T. C.; Klein, M. L. *Nano Lett.* **2009**, *9*, 537–541.
(19) Roxbury, D.; Manohar, S.; Jagota, A. *J. Phys. Chem. C* **2010**, *114*, 13267–13276.
(20) Alexiadis, A.; Kassinos, S. *Chem. Rev.* **2008**, *108*, 5014–5034.
(21) Reddy, S. Y.; Leclerc, F.; Karplus, M. *Biophys. J.* **2003**, *84*, 1421–1449.
(22) *Materials Studio (R)*; Accelrys Inc.: San Diego, CA, 2009.
(23) Humphrey, W.; Dalke, A.; Schulten, K. *J. Mol. Graphics* **1996**, *14*, 33–38.
(24) Berendsen, H. J. C.; van der Spoel, D.; van Drunen, R. *Comput. Phys. Commun.* **1995**, *91*, 43–56.
(25) Lindahl, E.; Hess, B.; van der Spoel, D. *J. Mol. Model.* **2001**, *7*, 306–317.
(26) van der Spoel, D.; Lindahl, E.; Hess, B.; Groenhof, G.; Mark, A. E.; Berendsen, H. J. C. *J. Comput. Chem.* **2005**, *26*, 1701–1718.
(27) Foloppe, N.; MacKerell, A. D. *J. Comput. Chem.* **2000**, *21*, 86–104.
(28) MacKerell, A. D., Jr.; Banavali, N. K. *J. Comput. Chem.* **2000**, *21*, 105–120.
(29) Jorgensen, W. L.; Chandrasekhar, J.; Madura, J. D.; Impey, R. W.; Klein, M. L. *J. Chem. Phys.* **1983**, *79*, 926.
(30) York, D. M.; Darden, T. A.; Pedersen, L. G. *J. Chem. Phys.* **1993**, *99*, 8345−8348.
(31) Manohar, S.; Mantz, A. R.; Bancroft, K. E.; Hui, C. Y.; Jagota, A.; Vezenov, D. V. *Nano Lett.* **2008**, *8*, 4365–4372.
(32) Rubinstein, M.; Colby, R. H. *Polymer Physics*; Oxford University Press: New York, 2003; p 54.
(33) Mamdouh, W.; Dong, M. D.; Xu, S. L.; Rauls, E.; Besenbacher, F. *J. Am. Chem. Soc.* **2006**, *128*, 13305–13311.
(34) Stofer, E.; Chipot, C.; Lavery, R. *J. Am. Chem. Soc.* **1999**, *121*, 9503–9508.
(35) Tinland, B.; Pluen, A.; Sturm, J.; Weill, G. *Macromolecules* **1997**, *30*, 5763–5765.